Acta Cryst. (1981). A**37**, 857–863

Joint X-ray and Neutron Data Refinement of Structural and Charge Density Parameters*

BY P. COPPENS, R. BOEHME, P. F. PRICE AND E. D. STEVENS

Chemistry Department, State University of New York at Buffalo, Buffalo, New York 14214, *USA*

(*Received* 24 *October* 1980; *accepted* 22 *April* 1981)

Abstract

A procedure for joint refinement of X-ray and neutron data is described in which structural, charge density and extinction parameters are adjusted simultaneously in order to arrive at the best least-squares solution with respect to all available diffraction data. This $X + N$ refinement is applied to previously collected low-temperature data on oxalic acid dihydrate, $C_2H_2O_4.2H_2O$, and results are compared with the X-ray-only refinement, and an X-ray refinement with neutron values for the hydrogen structural parameters. The $X + N$ model deformation density shows higher peak heights in the lone-pair regions than the X-ray-only model density and resembles more closely the $X–N$ deformation maps. Though the $X + N$ maps are more strongly model dependent, they contain less noise, provide an analytical description of the deformation density and, unlike the $X–N$ density, can be obtained in principle with a less than complete data set. The estimate of the goodness-of-fit for each of the data sets requires an apportioning of the joint parameters, which in this study is based on the relative magnitude of the least-squares derivatives.

Introduction

Several formalisms are presently being used for an analytical description of the electron distribution in a crystal. The most widely applied of these use atom-centered non-spherical density functions with adjustable population and radial dependence (*i.e.* Hirshfeld, 1977; Stewart, 1976; Hansen & Coppens, 1978).

The methods suffer from the drawback of correlation between structural and charge density parameters. The occupancy of a dipolar density function, for example, tends to correlate with positional parameters of the atom on which it is centered, and the same is true for quadrupole functions and anisotropic thermal parameters. The extent of this correlation depends on the data cut off and will be less severe when large numbers of high-order reflections, which contain a relatively small contribution from the valence electrons, are available. This correlation is especially pronounced for hydrogen atoms which scatter only weakly in the high-order region.

When neutron diffraction data are available, a procedure is often adopted in which hydrogen-atom parameters are kept constant at their neutron values. An alternative explored here is the simultaneous refinement of X-ray and neutron data in order to arrive at the best solution with regard to all diffraction data. The least-squares program *MAUDY* written for this purpose allows adjustment of structural, charge density and extinction parameters and is an extension of the previously described program for refinement of X-ray data only (Hansen & Coppens, 1978).

Combining two data sets

Several issues arise which are related to the simultaneous use of data sets from different origins. They are discussed below.

1. *Differences in data collection temperature*

Systematic differences between spherical-atom X-ray and neutron diffraction temperature factors have been traced to bias in the X-ray results resulting from the spherical-atom approximation. Such differences were especially pronounced in early studies which did not include many high-order reflections (Coppens, 1968); but should be less severe for extended data sets. Nevertheless, several more recent studies have shown discrepancies between X-ray and neutron atomic vibrational tensors. These are probably due to differences in either data collection temperature or differences in the background correction applied in the two experiments. The latter possibility, which includes

* *Electron Population Analysis of Accurate Diffraction Data.* X. Part IX: Coppens, Moss & Hansen (1980). In *Computing in Crystallography*, edited by R. Diamond, S. Ramaseshan & K. Venkatesan. Bangalore: Indian Academy of Sciences.

0567-7394/81/060857-07$01.00

differences in the amount of TDS counted with the Bragg peak, cannot be ruled out as discrepancies between temperature parameters have sometimes been observed in room-temperature studies (Craven & McMullan, 1979).

To account for such differences the adjustable parameters in the present treatment include a temperature scale factor k_T which multiplies the neutron temperature parameters such that

$$F_{\text{neutron}}(\mathbf{H}) = \sum_{n}^{\substack{\text{all}\\ \text{atoms}}} \{b_n \exp(2\pi i \mathbf{H}.\mathbf{r}_n) \times \exp(-2\pi^2 k_T \sum_i \sum_j U_{i,j,n,N} h_i h_j a_i^* a_j^*)\}. \quad (1a)$$

This expression is appropriate for a temperature factor difference in the 'high-temperature limit' in which the temperature factors are proportional to the absolute temperature. For most molecular crystals this limit is reached even at liquid-nitrogen temperature. The use of (1*a*) is mainly dictated by our previous experience with combined X-ray and neutron data sets (sulfamic acid, for example, see Bats, Coppens & Koetzle, 1977). We note, however, that other alternatives exist such as

$$F_{\text{neutron}}(\mathbf{H}) = \sum_{n}^{\substack{\text{all}\\ \text{atoms}}} \{b_n \exp(2\pi i \mathbf{H}.\mathbf{r}_n) \times \exp[-2\pi^2 \sum_i \sum_j (U_{i,j,n,N} + \Delta U_{i,j}) \times h_i h_j a_i^* a_j^*]\}, \quad (1b)$$

where $\Delta U_{i,j}$, common to all atoms, may be chosen to follow the symmetry transformations of U_{ij} for symmetry-equivalent atoms, or to be similarly oriented for all atoms in the unit cell. The latter case would apply, for example, if a systematic error were due to incorrect allowance for absorption or anisotropic extinction in the two data sets.

2. *Relative weighting of the X-ray and neutron data*

Since the error function minimized is equal to the weighted sum of the squared discrepancies between the observed and calculated F or F^2, the relative weighting of the two data sets influences their respective importance in the least-squares procedure. In this study the weights in each of the data sets are derived from the agreement between symmetry-related reflections combined with counting statistics plus a term accounting for the variation of the standard reflections (McCandlish, Stout & Andrews, 1975).

3. *Estimate of the goodness of fit*

The expression for the goodness of fit of the model to the observations is $\sum w\Delta^2/(n-s)$, where the Δ are the least-squares discrepancies, n is the number of observations and s the number of parameters. When two data sets are involved as in the present case it is of interest to evaluate the goodness of fit for each of the data sets in order to assess the adequacy of the model and the weighting schemes used in the analysis. This evaluation requires an estimate of the relative dependency of each of the parameters on the X-ray and neutron data sets. Information on this relative dependence is contained, of course, in the matrix **B** of the least-squares normal equations, the elements of which are the sums of the contributions from the X-ray and neutron observations

$$\mathbf{B} = \mathbf{B}_X + \mathbf{B}_N. \quad (2)$$

The required estimate may be based on the X-ray and neutron contributions to the diagonal elements of **B**, such that for each parameter u_j the fractional dependence φ is given by

$$\varphi_{X,j} = \frac{\sum_X w\left(\frac{\partial kE_c}{\partial u_j}\right)^2}{\sum_X w\left(\frac{\partial kE_c}{\partial u_j}\right)^2 + \sum_N w\left(\frac{\partial kE_c}{\partial u_j}\right)^2}; \quad \varphi_{N,j} = \frac{\sum_N w\left(\frac{\partial kE_c}{\partial u_j}\right)^2}{\sum_X w\left(\frac{\partial kE_c}{\partial u_j}\right)^2 + \sum_N w\left(\frac{\partial kE_c}{\partial u_j}\right)^2}, \quad (3)$$

where E is either F or F^2 depending on the function minimized. If a diagonal approximation were employed in the least-squares refinement, φ_X and φ_N would be inversely proportional to the squared standard deviations obtained in the X-ray or neutron data respectively. An alternative φ_X, based on the square root of the contribution to the diagonal elements $\{\sum_X w(\partial kE_c/\partial u_j)^2\}^{1/2}$, has also been considered. As it does not provide basically different insight it will not be further discussed here.

It can be readily shown that for a positional parameter $u_{i,n}$ of atom n and $E = F$ expression (3) may be approximated by

$$\varphi_X = n_X\langle w(h_i \bar{f}_n)^2\rangle / \{n_X\langle w(h_i \bar{f}_n)^2\rangle + n_N\langle w(h_i \bar{b}_n)^2\rangle\} \quad (4a)$$

while for a vibrational parameter U_{ij}:

$$\varphi_X = n_X\langle w(h_i h_j \bar{f}_n)^2\rangle / \{n_X\langle w(h_i h_j \bar{f}_n)^2\rangle + n_N\langle w(h_i h_j \bar{b}_n)^2\rangle\}, \quad (4b)$$

Table 1. *Information on X-ray and neutron data sets on oxalic acid dihydrate used in the present analysis*

	X-ray	Neutron
Reference	Stevens & Coppens (1980)	McMullen & Koetzle (1980)
sin θ/λ limits	$0{\cdot}0 < \sin\theta/\lambda < 1{\cdot}20$ Å^{-1}	$0{\cdot}0 < \sin\theta/\lambda < 1{\cdot}00$ Å^{-1}
Wavelength	0·7083 Å	0·8218 Å
Number of reflections measured including symmetry equivalents	4579	3797
Number of reflections after averaging of symmetry equivalents	2315	1912
Internal consistency factor*	0·024	0·031
Size of crystal used	0·41 × 0·27 × 0·42 mm	2·79 × 2·79 × 2·79 mm
Data collection temperature	100 ± 5 K†	100 K

* Defined as $\sum_{\mathbf{H}} \{F^2(\mathbf{H}) - \langle F^2(\mathbf{H})\rangle\}/\sum_{\mathbf{H}} F^2(\mathbf{H})$.

† Estimate of uncertainty in temperature measurement.

where n_X and n_N represent the number of X-ray and neutron observations and $\bar{f}$ and $\bar{b}$ are the thermally attenuated X-ray and neutron scattering factors respectively. Expressions (4*a*) and (4*b*) illustrate the effect of the number of reflections and their relative weighting, and the increasing importance of the neutron data in the high-angle region.

Application to low-temperature X-ray and neutron data on oxalic acid dihydrate

The joint refinement has been applied to a number of data sets including NaSCN (Bats, Coppens & Kvick, 1977), H_2O_2 (Savariault & Lehmann, 1980) and oxalic acid dihydrate (Stevens & Coppens, 1980). The results for the last compound have been analyzed in detail and will be reported here. The X-ray data were combined with neutron data collected at Brookhaven National Laboratory by McMullen & Koetzle (1980) as part of the electron density project of the Commission on Charge, Spin and Momentum Densities of the IUCr. Details on both data sets are given in Table 1, and the atom numbering is given in Fig. 1.

In addition to the joint X-ray and neutron refinement (refinement I), refinements with multipolar density functions were performed on the X-ray data only, first varying all atoms including hydrogen (refinement II) and secondly keeping the hydrogen positional and thermal parameters fixed at their neutron values (refinement III). A separate refinement of the neutron data was also done. Details and final R factors are listed in Table 2. The function minimized in all refinements is $\sum w_F(F_o - |kF_c|)^2$ where the weight w_F is derived from $w_{F^2} = 1/(\sigma_{F^2})^2$ as described by Rees (1976) and σ_{F^2} is estimated from

$$\sigma_{F^2} = \{\sigma^2_{\text{counting}} + (0{\cdot}02F^2)^2\}^{1/2}, \qquad (5)$$

the proportionality factor of 0·02 being derived from considerations described above. In the case of X-ray data σ_{F^2} was replaced by the standard deviation derived from the multiple observation of symmetry-related reflections if the latter exceeded the value calculated according to (5).

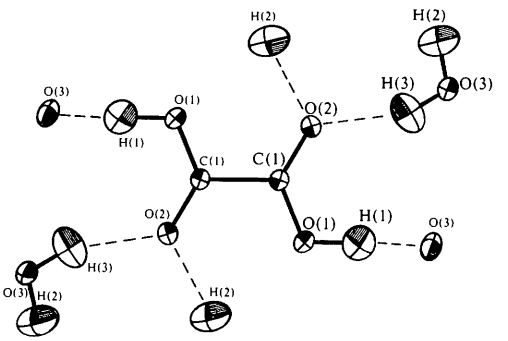

Fig. 1. Hydrogen bonding and numbering of the atoms in α-oxalic acid dihydrate. Thermal ellipsoids are 75% probability ellipsoids at 100 K.

Comparison of results

1. *Parameters and bond lengths*

The relative dependence of the structural parameters on the X-ray data in the joint refinement is listed in Table 3. The results show a pronounced influence of the X-ray and neutron scattering factors as predicted by expressions (4*a*) and (4*b*). The oxygen atom, which has a relatively small neutron scattering length (5·6 fm) and the largest X-ray scattering factor, is strongly dependent on the X-ray data, while the hydrogen-atom parameters are almost exclusively derived from the neutron measurements. Carbon, which is a stronger neutron and weaker X-ray scatterer than oxygen, has an 80% X-ray and 20% neutron dependence.

The final temperature scale parameter is 0·892 (2). This value is very close to the ratios of the equivalent isotropic temperature parameters from the neutron and X-ray only refinements, which are 0·880, 0·898, 0·898 and 0·902 for C, O(1), O(2) and O(3) respectively. As the neutron data were collected in a cryostat, while a gas flow system was used for the X-ray experiment, the neutron temperature measurement (100 K) is more likely to be correct. This would imply an X-ray data collection temperature of about 112 K if the dis-

Table 2. *Summary of least squares*

All X-ray refinements include multipoles up to the hexadecapole level.

	I Joint X-ray neutron		II X-ray only*	III Neutron only	IV X-ray with neutron values for hydrogen structural parameters†
	X-ray	Neutron			
$N_{observations}$	2117	3164‡	2118	3165‡	2117
$N_{variables}$	111·9§	39·1§	128	70	116
Scale factor	5·99 (1)	13·20 (2)	6·01 (1)	13·15 (2)	6·00 (1)
R (%)¶	1·39	3·77	1·34	3·62	1·35
R_w (%)¶	1·61	2·93	1·54	2·79	1·56
$\sum wA^2/(n-s)$	1·10	1·25	1·05	1·20	1·07
	1·13	1·32			
g_{11}, g_{iso}	13·6 (9) × 10^{-6}	6·4 (2) × 10^{-4}	14·0 (9) × 10^{-6}	6·5 (3) × 10^{-4}	13·8 (9) × 10^{-6}
g_{22}		3·9 (3) × 10^{-4}		4·8 (2) × 10^{-4}	
g_{33}		3·2 (2) × 10^{-4}		4·1 (2) × 10^{-4}	
g_{12}		−2·2 (2) × 10^{-4}		−2·4 (2) × 10^{-4}	
g_{13}		1·2 (2) × 10^{-4}		0·6 (2) × 10^{-4}	
g_{23}		−2·9 (2) × 10^{-4}		−3·5 (3) × 10^{-4}	

* Hydrogen atoms assigned isotropic vibrational parameters.

† Hydrogen temperature factors corrected by multiplication with temperature difference parameter from refinement I.

‡ Symmetry-related reflections not averaged to allow refinement of anisotropic extinction.

§ 63 parameters (nine for each of the seven atoms) are jointly determined by the X-ray and neutron data.

¶ Defined as $R = \sum (F_{obs} - |kF_{calc}|)/\sum F_{obs}$, $R_w = [\sum w(F_{obs} - |kF_{calc}|)^2/\sum F_{obs}^2]^{1/2}$; excluding reflections for which both F_{obs} and $F_{calc} < 3\sigma$.

crepancy is indeed fully to be attributed to a temperature difference. This result seems not unreasonable given the uncertainties in the absolute temperature measurement when using a gas flow system. We note that as bonding anisotropy has been incorporated in the X-ray scattering model and no residual bonding features remain, it cannot be a cause for the temperature parameter difference in this case.

For the heavy-atom positional and charge density parameters no significant differences are found between results from the joint refinement (I) and the X-ray-only multipole analysis (II). The latter do not show the positional parameter bias observed for the oxygen atoms in *p*-nitropyridine *N*-oxide (Hansen & Coppens, 1978). This different behavior may be related to the higher sin θ/λ cut-off in the oxalic acid data set. Even the hydrogen-atom charge density parameters from refinement II are in remarkable agreement with those from the joint refinement, although standard deviations are generally higher when neutron data are not used (Table 4). The expansion–contraction parameters κ' and κ'' for the hydroxylic hydrogen atom H(1) are an exception. They are too large, *i.e.* the H atom is too contracted while the isotropic hydrogen temperature parameter is too large by a factor 1·8 compared with the value from the joint refinement.

As shown in Table 5 the multipole refinement of X-ray data only does not give reliable O—H bond lengths; the values obtained differ by 0·03–0·05 Å from the true distances.

Table 3. *Relative dependence (in %) of joint parameters on X-ray data calculated according to expression* (3)

	x	y	z	U_{11}	U_{22}	U_{33}	U_{12}	U_{13}	U_{23}
C(1)	83	80	80	81	75	79	83	81	83
O(1)	91	90	89	89	86	88	90	89	89
O(2)	91	90	90	90	86	87	90	89	89
O(3)	91	88	90	90	87	88	90	90	89
H(1)	2	2	2	1	1	1	1	1	1
H(2)	4	4	3	2	3	2	2	3	2
H(3)	4	4	4	2	2	2	2	2	2

Table 4. *Hydrogen-atom charge density parameters*

The density expression for the hydrogen atom is

$$\rho_H(\mathbf{r}) = \rho_{core}(\mathbf{r}) + P_{val}\rho_{val}(\kappa'\mathbf{r}) + P_{10}\rho_{10}(\kappa''\mathbf{r}) + P_{20}\rho_{20}(\kappa''\mathbf{r})$$

(Hansen & Coppens, 1978).

Refinement	I Joint X, N		II X only	
	H(1)	H(2), H(3)*	H(1)	H(2), H(3)*
κ'	1·08 (2)	1·15 (2)	1·21 (9)	1·15 (4)
κ''	1·07 (7)	0·82 (3)	1·37 (19)	0·80 (5)
P_v	0·78 (3)	0·88 (3)	0·75 (4)	0·95 (4)
P_{10}†	0·066 (7)	0·193 (16)	0·098 (12)	0·21 (2)
P_{20}†	0·08 (1)	0·11 (1)	0·11 (2)	0·09 (2)
U_{iso} (Å²)‡	0·0260	0·0304, 0·0342	0·048 (8)	0·031 (3), 0·033 (3)

* The two hydrogen atoms on the water molecule have been constrained to have identical charge density parameters.

† The local z axes point along the O—H vector.

‡ Equivalent isotropic temperature parameters for refinement I.

Table 5. *Comparison of bond lengths* (Å) *from different refinements* (*see Table* 2 *for definition of the refinements*)

	I	II	III	IV
C–C	1·5427 (3)	1·5418 (3)	1·5448 (5)	1·5417 (3)
C–O(1)	1·2874 (3)	1·2874 (3)	1·2872 (4)	1·2876 (3)
C–O(2)	1·2232 (2)	1·2238 (2)	1·2221 (4)	1·2238 (2)
O(1)–H(1)	1·0691 (8)	1·12 (2)	1·0686 (8)	1·0691 (2)
O(3)–H(2)	0·9705 (8)	0·93 (3)	0·9701 (8)	0·9707 (2)
O(3)–H(3)	0·9659 (8)	0·93 (3)	0·9665 (8)	0·9663 (1)

2. *Density maps*

A further intercomparison of the different approaches is based on the deformation density maps. Several sections through the oxalic acid dihydrate crystals contain chemically interesting features, including those through the oxalic acid and water molecules and the section bisecting the two water O–H bonds, which are used here for the comparison of different types of density maps.

We define the following charge density deformation maps:

1. $X-(X+N)$ (dynamic) deformation density:

$$\rho(\mathbf{r})=\frac{1}{V}\sum (F_{\rm obs}-F_{\rm calc})\exp -2\pi i\mathbf{H}.\mathbf{r},$$

where $F_{\rm calc}$ is calculated with the parameters from the joint refinement and spherical-atom form factors.

2. $X-N$ (dynamic) deformation density as 1 but with $F_{\rm calc}$ obtained with the neutron parameters (after scaling of temperature parameters to X-ray values).

3. $X+N$ (dynamic) model density:

$$\rho(\mathbf{r})=\frac{1}{V}\sum (F_{\rm calc,model}-F_{\rm calc,spherical\,atom})\times\exp -2\pi i\mathbf{H}.\mathbf{r},$$

where $F_{\rm calc,model}$ are the structure factors calculated in the joint X,N multipole model refinements.

4. X (dynamic) model density as 3 but with multipole and structural parameters from X-ray-only refinement (except for hydrogen structural parameter for which neutron data have been used).

5. $X+N$ (static) model density:

$$\rho(\mathbf{r})=\sum_i P_i\,\psi_i-\sum \rho_{\rm spherical\,atom},$$

where P_i and ψ_i are the populations and static density functions from the joint $X+N$ refinement.

6. X (static) model density as 5 but with populations and functions from X-ray-only refinements.

A number of the density maps are reproduced in Fig. 2, while peak heights in the bond and lone-pair regions in experimental and theoretical maps (Stevens, 1980) are listed in Table 6.

Comparison of the dynamic X and $X+N$ model densities (4 and 3) shows the lone-pair peak heights to be systematically too low in the former, while the $X+N$ model peak heights are only slightly lower than those in the model-independent $X-N$ density. Two theoretical maps are available for comparison either in their static or their dynamic version. The 4-31 G maps are biased by basis-set truncation, but this effect should be much less severe in the extended basis set (EBS) results, which still show higher lone-pair peak heights than obtained from experiment. Quite reasonable agreement is obtained, however, for the peak heights in the bond regions.

The discrepancy in the lone-pair peak heights is largest for the X model map and smallest for the X–N density. It should be kept in mind, however, that, apart from remaining basis-set truncation effects in the theory, full agreement cannot be expected, as the effect of intermolecular interactions is not accounted for in the theoretical results. The discrepancies are much increased in the corresponding 'static' maps. Undoubtedly approximations implied in extrapolating the limited resolution dynamic map to an apparent 'infinite resolution' 'static density' contribute to these differences.

The X–N map, which is much less model dependent,* may be a more objective representation of the deformation density than any of the model maps, even though the differences with the $X+N$ density are small, especially when peak *heights* are considered. The advantages of the model maps, and in particular those obtained from the $X+N$ refinement, are that they do not suffer from experimental noise, and provide an analytical description of the deformation density which may be used in the calculation of derived properties.

For acentric structures the multipole refinement provides an estimate of the phases of the observed structure factors as discussed for the X-ray-only case by Thomas (1978) and Mullen (1980). If the criterion is used that the best estimate of the phases is obtained from the model that produces the fewest features in the residual density difference map (Coppens, 1974), it may be argued that the X-ray-only refinement is, for this purpose, superior to the $X+N$ procedure, which is constrained by the neutron data. In any case X–N maps obtained with 'observed' phases from either method should be superior to those based on the straight algebraic difference in the calculation of ΔF. It must be noted, however, that such X–N maps are no longer model independent.

* As pointed out by a referee the X–N map is model dependent to the extent that the scale and extinction parameters are influenced by the scattering model.

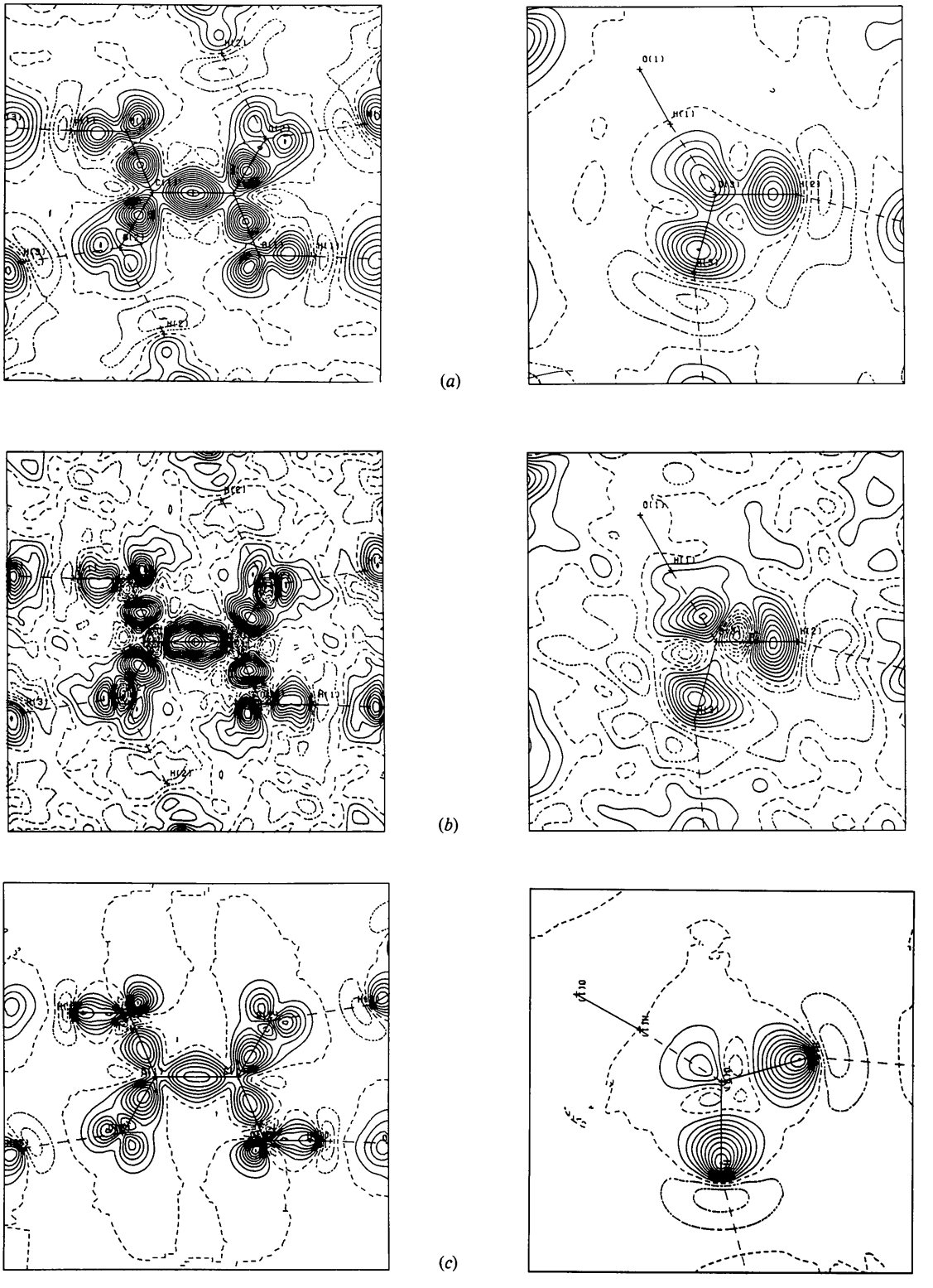

Fig. 2. Density maps in the oxalic acid (left) and water molecule (right) planes. Zero and negative contours broken. (*a*) $X + N$ dynamic model density. Contours at 0·05 e Å^{-3}. (*b*) X–N deformation density. Contours as in (*a*). (*c*) $X + N$ static model density. Contours at 0·10 e Å^{-3}.

Table 6. *Summary of bond and lone-pair peak heights* (e Å^{-3}) *in experimental and theoretical electron density maps*

	Experimental			Theoretical	
Dynamic density	$X+N$ model	X model	$X-N$	4-31G	EBS
C(1)–C(1′)	0·57	0·57	0·69	0·38	0·58
C(1)–O(1)	0·47	0·48	0·49	0·20	0·43
C(1)–O(2)	0·59	0·62	0·55	0·46	0·62
O(1)–H(1)	0·35	0·33	0·33	0·23	0·40
O(1) l.p.	0·45	0·37	0·49	0·73	0·60
O(2) l.p.	0·35	0·28	0·41	0·61	0·53
O(2) l.p.	0·29	0·25	0·31	0·64	0·53
Static density					
C(1)–C(1′)	0·64	0·65		0·40	0·67
C(1)–O(1)	0·58	0·60		0·25	0·54
C(1)–O(2)	0·79	0·85		0·54	0·70
O(1)–H(1)	0·62	0·55		0·34	0·56
O(1) l.p.	0·93	0·68		1·18	1·10
O(2) l.p.	0·61	0·44		1·49	1·22
O(2) l.p.	0·54	0·42		1·39	1·32

The authors would like to thank Drs Koetzle and McMullen from Brookhaven National Laboratory for making the neutron data on oxalic acid dihydrate available. Support of this work by the National Science Foundation (CHE7905897) is gratefully acknowledged.

References

BATS, J. W., COPPENS, P. & KOETZLE, T. F. (1977). *Acta Cryst.* B**33**, 37–45.
BATS, J. W., COPPENS, P. & KVICK, A. (1977). *Acta Cryst.* B**33**, 1534–1542.
COPPENS, P. (1968). *Acta Cryst.* B**24**, 1272–1274.
COPPENS, P. (1974). *Acta Cryst.* B**30**, 255–261.
COPPENS, P., MOSS, G. & HANSEN, N. K. (1980). In *Computing in Crystallography*, edited by R. DIAMOND, S. RAMASESHAN & K. VENKATESAN. Bangalore: Indian Academy of Sciences.
CRAVEN, B. M. & MCMULLAN, R. K. (1979). *Acta Cryst.* B**25**, 934–945.
HANSEN, N. K. & COPPENS, P. (1978). *Acta Cryst.* A**34**, 909.
HIRSHFELD, F. L. (1977). *Isr. J. Chem.* **16**, 226–231.
MCCANDLISH, L. E., STOUT, G. H. & ANDREWS, L. C. (1975). *Acta Cryst.* A**31**, 245–249.
MCMULLEN, R. K. & KOETZLE, T. F. (1980). Unpublished results.
MULLEN, D. (1980). *Acta Cryst.* B**36**, 1610–1615.
REES, B. (1976). *Acta Cryst.* A**32**, 483–488.
SAVARIAULT, J. M. & LEHMANN, M. S. (1980). *J. Am. Chem. Soc.* **102**, 1298–1307.
STEVENS, E. D. (1980). *Acta Cryst.* B**36**, 1876–1887.
STEVENS, E. D. & COPPENS, P. (1980). *Acta Cryst.* B**36**, 1864–1876.
STEWART, R. F. (1976). *Acta Cryst.* A**32**, 565–574.
THOMAS, J. O. (1978). *Acta Cryst.* A**34**, 819–823.

Acta Cryst. (1981). A**37**, 863–871

Direct Observation of TDS Profiles from Perfect Silicon Single Crystals on a Neutron Diffractometer

BY HANS A. GRAF AND JOCHEN R. SCHNEIDER

Hahn-Meitner-Institut für Kernforschung, Glienicker Strasse 100, *D*-1000 *Berlin* 39, *Federal Republic of Germany*

AND ANDREAS K. FREUND AND MOGENS S. LEHMANN

Institut Max von Laue–Paul Langevin, 156*X*, *F*-38042 *Grenoble CEDEX, France*

(*Received* 9 *January* 1981; *accepted* 5 *May* 1981)

Abstract

TDS profiles convoluted with the instrument resolution were obtained by forming differences between diffraction profiles measured with neutrons of wavelength 0·60 Å on three perfect Si crystals of different thickness. The profiles were measured with two detector apertures for the reflections 022, 004, 044, 026, 008 and 066. From these measurements TDS correction factors α and hence a correction term ΔB for the temperature parameter of Si were derived. The temperature parameter of Si was determined for two temperatures, 92 and 292 K, as $B_{92} = 0{\cdot}212\ (3)$ Å^2 and $B_{292} = 0{\cdot}422\ (3)$ Å^2, respectively, from the refinement of 100 symmetry-inequivalent reflections measured with neutrons of wavelength 0·53 Å on an imperfect Si crystal.

0567-7394/81/060863-09$01.00